



ISTITUTO NAZIONALE DI RICERCA METROLOGICA Repository Istituzionale

Density Measurements of an Air-Like Binary Mixture over the Temperature Range from 100 K to 298.15 K at Pressures up to 8.0 MPa

Original

Density Measurements of an Air-Like Binary Mixture over the Temperature Range from 100 K to 298.15 K at Pressures up to 8.0 MPa / von Preetzmann, Nils; Kleinrahm, Reiner; Eckmann, Philipp; Cavuoto, Giuseppe; Richter, Markus. - In: INTERNATIONAL JOURNAL OF THERMOPHYSICS. - ISSN 0195-928X. - 42:9(2021). [10.1007/s10765-021-02871-4]

Availability:

This version is available at: 11696/80400 since: 2024-03-05T10:14:49Z

Publisher:

Springer

Published

DOI:10.1007/s10765-021-02871-4

Terms of use:

This article is made available under terms and conditions as specified in the corresponding bibliographic description in the repository

Publisher copyright

SPRINGER NATURE OPEN ACCESS

This article is licensed under a Creative Commons Attribution 4.0 International License, which permits use, sharing, adaptation, distribution and reproduction in any medium or format, as long as you give appropriate credit to the original author(s) and the source, provide a link to the Creative Commons licence, and indicate if changes were made. The images or other third party material in this article are

(Article begins on next page)



Density Measurements of an Air-Like Binary Mixture over the Temperature Range from 100 K to 298.15 K at Pressures up to 8.0 MPa

Nils von Preetzmann¹ · Reiner Kleinrahm¹ · Philipp Eckmann² · Giuseppe Cavuoto³ · Markus Richter²

Received: 11 May 2021 / Accepted: 19 May 2021 / Published online: 24 June 2021
© The Author(s) 2021

Abstract

Densities of an air-like binary mixture (0.2094 oxygen + 0.7906 nitrogen, mole fractions) were measured along six isotherms over the temperature range from 100 K to 298.15 K at pressures up to 8.0 MPa, using a low-temperature single-sinker magnetic suspension densimeter. The measurements were carried out at $T=(100, 115, \text{ and } 130)$ K in the homogeneous gas and liquid region, and at $T=(145, 220, \text{ and } 298.15)$ K in the supercritical region (critical temperature $T_C=132.35$ K); in total, we present results for 52 (T, p) state points. The relative expanded combined uncertainty ($k=2$) of the experimental densities was estimated to be between 0.03 % and 0.13 %, except for four values near the critical point. The largest error is caused by the magnetic suspension coupling in combination with the mixture component oxygen, which is strongly paramagnetic; the resulting force transmission error is up to 1.1 %. However, this error can be corrected with a proven correction model to an uncertainty contribution in density of less than 0.044 %. Due to a supercritical liquefaction procedure and the integration of a special VLE-cell, it was possible to measure densities in the homogeneous liquid phase without changing the composition of the liquefied mixture. Moreover, saturated liquid and saturated vapor densities were determined at $T=(100, 115, \text{ and } 130)$ K by extrapolation of the experimental single-phase densities to the saturation pressure. The new experimental results were compared with the mixture model of Lemmon *et al.* for the system (nitrogen + argon + oxygen) and the GERG-2008 equation of state.

Keywords Air-like binary mixture · Cryogenic state · Density measurement · Liquefied air · Magnetic suspension coupling · Single-sinker densimeter

✉ Markus Richter
m.richter@mb.tu-chemnitz.de

Extended author information available on the last page of the article

1 Introduction

The gas mixture in the earth's atmosphere is known to be air. It mainly consists of the two gases nitrogen and oxygen but also contains argon, carbon dioxide, and traces of other gases. Air without water vapor is called dry air. The ternary mixture composed of approximately 0.78 mol fraction nitrogen, about 0.21 mol fraction oxygen, and roughly 0.01 mol fraction argon is often considered to be standard dry air. In the present work, we examined the (p, ρ, T) behavior of a simplified standard dry air mixture consisting of 0.7906 mol fraction nitrogen and 0.2094 mol fraction oxygen. For this binary mixture, accurate data over large temperature and pressure ranges are particularly useful for performance testing and the development of binary-specific parameters and departure functions in contemporary multi-component mixture models. This is not only of interest in science but in conjunction with other relevant binary mixtures also important for practical applications such as cryogenic air separation and direct air capture.

In the field of thermodynamic property research, the density measurements of the given air-like binary mixture are also valuable for checking an empirical model [1, 2] which was specifically developed to correct the so-called force transmission error caused by a magnetic suspension coupling, as it is integrated in our single-sinker densimeter. Since one of the two force transmission errors, the so-called fluid-specific effect, is very large in case of oxygen as a component in a fluid mixture (see Sect. 2.2), the air-like binary mixture studied here is very suitable for verifying the correction model.

In our previous papers, we already presented density data for six liquefied natural gases [3, 4], nine liquefied methane-rich binary mixtures [5, 6] and two liquefied biomethane-like mixtures [7]. In the present paper, we report the results of accurate density measurements of an air-like mixture (0.2094 oxygen + 0.7906 nitrogen, mole fractions) over the temperature range from 100 K to 298.15 K at pressures up to 8.0 MPa. The apparatus utilized for density measurements is a special single-sinker densimeter for cryogenic liquid mixtures. The new experimental results were compared with the mixture model of Lemmon *et al.* [8] for the system (nitrogen + argon + oxygen) and additionally with the GERG-2008 equation of state [9, 10].

2 Experimental Section

2.1 Apparatus Description

The density measurements reported in this paper were carried out with a precision densimeter, which was deliberately designed for accurate density measurements of cryogenic liquid mixtures, such as LNG; it covers a temperature range from 90 K to 300 K at pressures up to 12 MPa. A single-sinker densimeter, based on the Archimedes (buoyancy) principle, in conjunction with a magnetic suspension

coupling is utilized. The design of the cryogenic densimeter, the temperature and pressure measurement, and the implementation of a special “VLE-cell” as a novel feature were described in detail by Richter *et al.* [3] in 2016. Two schematic diagrams presented in their work, which illustrate the measuring principle and the design of the densimeter, are shown in Sect. S1 of the Online Resource of this paper. In one of our latest papers [5], we presented improvements of the design to reduce diffusion effects and the force transmission error (FTE) of the magnetic suspension coupling [1, 2]. In the following, we only summarize the description of the apparatus presented by Richter *et al.* [3]. Overviews of this general type of densimeter were provided by Wagner and Kleinrahm [11] as well as by McLinden [12].

The single-sinker method basically allows an absolute determination of the fluid density. This method is applied in conjunction with a magnetic suspension coupling and a load compensation mechanism (differential method). A sinker of known volume $V_S(T, p)$ and known mass m_S (in the present case: a single-crystal silicon, $m_S \approx 60.95$ g, $V_S \approx 26.17$ cm³, $\rho_S \approx 2.329$ g·cm⁻³) is weighed while immersed in the fluid of interest inside a pressure-tight measuring cell. Thus, the result of weighing the sinker located in the fluid, $m_{S,\text{fluid}}^*$, is the difference between the mass of the sinker and the buoyancy of the fluid:

$$m_{S,\text{fluid}}^* = m_S - \rho_{\text{fluid}} \cdot V_S(T, p), \quad (1)$$

where ρ_{fluid} denotes the fluid density. When weighing the sinker inside the evacuated measuring cell via the magnetic suspension coupling, the weighing result is not the mass of the sinker, m_S , but a minimally different result, $m_{S,\text{vac}}^*$, due to a small FTE of the magnetic suspension coupling [1, 2]. Rearranging Eq. 1 yields the fluid density:

$$\rho_{\text{fluid}} = \frac{m_{S,\text{vac}}^* - m_{S,\text{fluid}}^*}{V_S(T, p)}. \quad (2)$$

Equation (2) actually requires additional terms since essential details of the measurement procedure (e.g., the correction of the FTE) have to be taken in account, as discussed in Appendix A1 of the paper by Richter *et al.* [3]. Moreover, the problem of the FTE due to the magnetic suspension coupling is described in detail by Kleinrahm *et al.* [2]. Since the FTE has a significant influence on the accuracy of density measurements in case of oxygen-containing fluids, the FTE is explained and discussed in the next section.

For the measurement of fluid densities, the sinker is connected to an analytical balance (readability: 0.01 mg) employing an appropriate coupling and decoupling device. Gravity and buoyancy forces acting on the sinker are transmitted to the balance via the magnetic suspension coupling, which isolates the fluid sample (which may be at high pressure and very low temperature) from the balance that is at ambient conditions. For compensation of the balance’s zero-point drift, the weighing procedure considers the small drift of the balance reading in the tare position by subtracting it from the balance reading in the measuring position. The balance is operated near its tare point using a load compensation mechanism to reduce possible

errors of the balance due to changes in the slope of the characteristic curve over the weighing range.

Since balances are generally calibrated in air with internal standard masses, they will read “100.00000 g” when weighing a 100 g standard mass, even though the weighing is affected by air buoyancy. The balance calibration factor α accounts for this fact:

$$\alpha = 1 / (1 - \rho_{\text{air}} / \rho_{\text{calib}}), \quad (3)$$

where $\alpha \approx 1.000150$ for a typical sea-level air density of $\rho_{\text{air}} \approx 1.20 \text{ kg}\cdot\text{m}^{-3}$, and stainless-steel calibration masses with a density of $\rho_{\text{calib}} \approx 8000 \text{ kg}\cdot\text{m}^{-3}$. Therefore, this fact has been taken into account and inserted into Eq. 2, which yields:

$$\rho_{\text{fluid}} = \frac{(m_{\text{S,vac}}^* - m_{\text{S,fluid}}^*) / \alpha}{V_{\text{S}}(T, p)}. \quad (4)$$

Hence, the density values calculated with Eq. 2 become smaller by about 0.0150 %.

2.2 Force Transmission Error (FTE) Due to the Magnetic Suspension Coupling

The force transmission error due to the magnetic suspension coupling can be subdivided into two parts: an apparatus contribution, ε_{vac} , and a fluid contribution, ε_{fse} , which is called the “fluid-specific effect.” In order to correct the influence of the FTE on density measurement and, thus, to reduce the uncertainty, Eq. 4 can be extended by the term $(1 + \varepsilon_{\text{vac}} + \varepsilon_{\text{fse}})^{-1}$ to

$$\rho_{\text{fluid}} = \frac{(m_{\text{S,vac}}^* - m_{\text{S,fluid}}^*) / \alpha}{V_{\text{S}}(T, p)} \cdot (1 + \varepsilon_{\text{vac}} + \varepsilon_{\text{fse}})^{-1}, \quad (5)$$

which yields the final equation for determining the fluid density. For most applications, the last term in Eq. 5 can be slightly simplified and replaced by $(1 - \varepsilon_{\text{vac}} - \varepsilon_{\text{fse}})$, because $|\varepsilon_{\text{vac}}| \ll 1$ and $|\varepsilon_{\text{fse}}| \ll 1$ for most fluid mixtures; then, $1 / (1 + \varepsilon_{\text{vac}} + \varepsilon_{\text{fse}}) \approx (1 - \varepsilon_{\text{vac}} - \varepsilon_{\text{fse}})$. This simplification was often used in our previous papers [3–7]. However, it cannot be used in the present case because the values for ε_{fse} are too large for fluid mixtures containing more than a few mole % of oxygen. The derivation of Eq. 5, the explanation of the FTE, and the determination of the two FTE contributions, ε_{vac} and ε_{fse} , are explained in detail by Kleinrahm *et al.* [2]. Nevertheless, the most important relationships are briefly explained below.

2.2.1 Apparatus Contribution of the FTE

The apparatus contribution of the FTE, which we term ε_{vac} , is caused by the magnetic properties of the coupling housing, as well as by the magnetic components in its vicinity. When the sinker in the measuring cell is lifted by the magnetic

suspension coupling for a density measurement, the position of the permanent magnet changes by a few millimeters from the lower tare position to the upper measuring position (see Fig. S1 in Online Resource). Therefore, the force interaction between the permanent magnet and the coupling housing changes, which causes the FTE of the coupling housing. For the determination of the value of ε_{vac} , the density sinker was carefully weighed in the evacuated measuring cell via the magnetic suspension coupling. This yields the value $m_{\text{S,vac}}^*$, and ε_{vac} can be determined by

$$\varepsilon_{\text{vac}} = \left(m_{\text{S,vac}}^* / \alpha - m_{\text{S}} \right) / m_{\text{S}}. \quad (6)$$

The magnitude of the apparatus contribution of the FTE, ε_{vac} , depends on the magnetic properties of the material of the coupling housing and of its surrounding components; the values are positive for diamagnetic and negative for paramagnetic materials. These facts are described in more detail in Annotation 3 of Appendix A1 of the paper by Kleinrahm *et al.* [2]. The measuring cell (with integrated coupling housing) of our densimeter (see Online Resource, Sect. S1, Fig. S1) was made of a beryllium copper alloy (CuBe2) which is very slightly diamagnetic [3, 5]. Therefore, the apparatus contribution of our single-sinker densimeter is likewise very small, namely, $\varepsilon_{\text{vac}}(T) = (+12, +13, +14, +14, +17, \text{ and } +19) \times 10^{-6}$ at $T = (100, 115, 130, 145, 220, \text{ and } 298.15)$ K, respectively; its expanded uncertainty ($k=2$) was estimated to be 4×10^{-6} .

2.2.2 Fluid Contribution of the FTE (Fluid-Specific Effect)

Like metals, fluids also have magnetic properties. Therefore, the magnetic field of the magnetic suspension coupling is influenced by the sample fluid inside the coupling housing. Due to the movement of the permanent magnet from the tare position to the measuring position, the force interaction between the permanent magnet and the coupling housing changes, which consequently affects the weighing result. The fluid contribution of the FTE is approximately proportional to the specific magnetic susceptibility of the fluid and, in addition, proportional to the change in position of the permanent magnet between the lower tare position and the upper measuring position (see Fig. S1 in Online Resource). This change of a few millimeters is represented by the density of the sinker minus the density of the sample fluid.

Hence, the fluid contribution of the FTE for single-sinker densimeters, represented by the so-called “fluid-specific effect,” ε_{fse} , can be calculated by

$$\varepsilon_{\text{fse}} = \varepsilon_{\rho} \cdot \left(-\frac{\chi_{\text{S}}}{\chi_{\text{S},0}} \right) \cdot \left(\frac{\rho_{\text{S}}}{\rho_0} - \frac{\rho_{\text{fluid}}}{\rho_0} \right), \quad (7)$$

where $\varepsilon_{\rho} = (53 \pm 2) \times 10^{-6}$ is an apparatus-specific constant (see next section), χ_{S} is the specific magnetic susceptibility of the sample fluid, $\chi_{\text{S},0} = 10^{-8} \text{ m}^3 \cdot \text{kg}^{-1}$ is a reducing constant, $\rho_{\text{S}} = 2329 \text{ kg} \cdot \text{m}^{-3}$ is the density of the silicon sinker, ρ_{fluid} is the density of the sample fluid, and $\rho_0 = 1000 \text{ kg} \cdot \text{m}^{-3}$ is also a reducing constant; see Kleinrahm *et al.* [2]. The expanded uncertainty ($k=2$) of this correction model, represented by

the term ε_{fse} , was estimated to be 4.0 %. The application of the model is explained in Sect. 2.2.4.

2.2.3 Apparatus-Specific Constant

The apparatus-specific constant, ε_ρ , (see Eq. 7) of our densimeter was provisionally determined for the first time by Richter *et al.* [3] in 2016; the result was $\varepsilon_\rho = (50 \pm 10) \times 10^{-6}$. After successful improvements of the densimeter, the constant was re-determined by Lentner *et al.* [5] in 2020 with the result $\varepsilon_\rho = (54 \pm 5) \times 10^{-6}$. Within this work the apparatus-specific constant of our densimeter was again re-determined through density measurements of the air-like binary mixture (0.2094 oxygen + 0.7906 nitrogen, mole fractions) at $T = 298.15$ K in the pressure range from 8.00 MPa to 0.40 MPa. The method for determining ε_ρ is explained by Kleinrahm *et al.* [2]. Our new result is $\varepsilon_\rho = (53 \pm 2) \times 10^{-6}$, where the last value in parentheses is the estimated expanded uncertainty ($k=2$). The apparatus-specific constant, ε_ρ , is not temperature dependent [1, 2]; this is shown and discussed in Sect. 3.3 for the isotherms at $T = (100, 115, 130, 145, 220, \text{ and } 298.15)$ K. Since the constant ε_ρ was determined with the same gas mixture that was studied here and, in addition, we were able to check this value in the temperature range from 100 K to 298.15 K, its uncertainty is smaller than in our previous papers [3–7]. Moreover, the expanded uncertainty ($k=2$) of the correction model, represented by the term ε_{fse} in Eq. 7, was estimated to be 4.0 %, which was larger in our earlier works [3–7]; this reduction is due to the reduced uncertainty of the apparatus-specific constant. We would like to expressly point out that the specified small uncertainties for the apparatus-specific constant and the correction model only apply in the present case for the density measurements of an air-like binary mixture. As additional information, we would like to mention here that the apparatus-specific constant, ε_ρ , can also be determined accurately by density measurement on pure oxygen, e.g., this was carried out by Lozano-Martín *et al.* [13]. Most densimeters, however, are not designed to measure pure oxygen and do not meet the corresponding safety requirements.

2.2.4 Magnetic Susceptibility of Fluids

Most common pure fluids are diamagnetic, e.g., nitrogen has a specific magnetic susceptibility of $\chi_s/\chi_{s0} \approx -0.54$ (negative values for diamagnetic substances) at $T \approx 293.15$ K, where $\chi_{s0} = 10^{-8} \text{ m}^3 \cdot \text{kg}^{-1}$ is a reducing constant; several typical examples are described in the Online Resource in Sect. S2.1. The susceptibility of diamagnetic fluids varies only slightly with temperature or not at all [14] (CRC Handbook 2016). In contrast to diamagnetic fluids, the susceptibility of paramagnetic fluids (positive values) is much greater and shows a much stronger temperature dependence, varying roughly as $1/T$. The most common paramagnetic fluids are oxygen and oxygen-containing mixtures, in particular air. The specific susceptibilities of oxygen and air are given in the Online Resource in Sect. S2.2. For example, the specific susceptibility of oxygen at $T = (293.15 \text{ and } 100)$ K is $\chi_s/\chi_{s0} = (+134.13 \text{ and } +393.20)$, respectively, and for an air-like binary mixture (0.2094 oxygen + 0.7906 nitrogen, mole fractions) at the same temperatures it is $\chi_s/\chi_{s0} = (+30.74 \text{ and } +90.82)$. An equation for calculating the

specific susceptibility of gas mixtures is described in the Online Resource in Sect. S2.1. It should be mentioned here that the susceptibility of oxygen does not only depend on temperature but also on its density; this behavior is briefly described in Sect. 2.2.5.

In the following, a few examples are intended to illustrate the fluid-specific effect. In case of diamagnetic fluids, the fluid contribution of the FTE is usually relatively small, e.g., $\varepsilon_{\text{fse}} \approx +50 \times 10^{-6}$ for pure nitrogen at a density $\rho_{\text{N}_2} = 600 \text{ kg}\cdot\text{m}^{-3}$, and it is not dependent on temperature. For a (paramagnetic) air-like binary mixture (0.2094 oxygen + 0.7906 nitrogen, mole fractions), however, the fluid contribution of the FTE is relatively large, e.g., $\varepsilon_{\text{fse}} \approx -7415 \times 10^{-6}$ at $T = 100 \text{ K}$ and $\rho_{\text{air}} \approx 794 \text{ kg}\cdot\text{m}^{-3}$ ($p \approx 8.0 \text{ MPa}$) and $\varepsilon_{\text{fse}} \approx -3580 \times 10^{-6}$ at $T = 298.15 \text{ K}$ and $\rho_{\text{air}} \approx 94 \text{ kg}\cdot\text{m}^{-3}$ ($p \approx 8.0 \text{ MPa}$); see Online Resource, Sect. S2.4, and Table S1. Hence, due to the uncertainty of the FTE correction model, the remaining influence of this FTE on the expanded uncertainty ($k=2$) of the experimentally determined densities is 4 % of the ε_{fse} values, which results in uncertainty contributions ($k=2$) between about 0.014 % and 0.045 %. In this context, we would like to mention that a significant fluid-specific effect also occurs when the densimeter and the measuring cell have been opened for test measurements, i.e., when there is air in the measuring cell under ambient conditions. For example, when the density sinker ($m_s \approx 60.95 \text{ g}$, $\rho_s \approx 2.329 \text{ g}\cdot\text{cm}^{-3}$, see Sect. 2.1) is weighed, the fluid-specific effect is $\varepsilon_{\text{fse}} \approx -0.37 \%$; see Online Resource, Sect. S2.4, and Table S1 for comparison.

2.2.5 Density Dependence of the Susceptibility of Oxygen

Unfortunately, the specific susceptibility of oxygen also depends on its density, which reduces its susceptibility. Therefore, the susceptibility of an oxygen-containing mixture, e.g., the air-like binary mixture (0.2094 oxygen + 0.7906 nitrogen, mole fractions) as studied here, also depends on density due to the influence of the partial density of oxygen. The magnitude of this effect and its influence on the uncertainty of our density measurements is discussed in the Online Resource in Sections S2.3 and S2.4. Since the magnitude of the effect is not well known, we roughly estimated an approximation term that describes the influence of the density of oxygen on the susceptibility of oxygen and on our air-like binary mixture. For low air densities, the influence on the measured values is negligible; however, it is up to +0.18 % at $T = 100 \text{ K}$ and $\rho_{\text{air}} \approx 794 \text{ kg}\cdot\text{m}^{-3}$ ($p \approx 8.0 \text{ MPa}$); in this case, the roughly estimated uncertainty of the approximation term results in an uncertainty contribution ($k=2$) in density of 0.059 %.

The fluid-specific effect, ε_{fse} , for our air-like binary mixture, including the estimated influence of the partial density of oxygen in our binary mixture on its susceptibility and, thus, on the fluid-specific effect, is explained in the Online Resource in Sect. S2.4 and listed in Table S1.

2.3 Experimental Material

The air-like binary mixture (0.2094 oxygen + 0.7906 nitrogen, mole fractions) was supplied in a steel cylinder with an internal volume of 50 dm^3 by Air Liquide, Germany; the initial pressure of the gas was 20 MPa. Its composition was

given as (0.205 ± 0.005) mole fraction oxygen in nitrogen, and the impurities in the gas mixture were given as follows: $x(\text{H}_2\text{O}) < 2.0 \times 10^{-6}$, $x(\text{CO}) < 1.0 \times 10^{-6}$, $x(\text{CO}_2) < 1.0 \times 10^{-6}$, $x(\text{C}_m\text{H}_n) < 0.1 \times 10^{-6}$.

To reduce the relatively large uncertainty in the composition of the gas mixture, we measured the density of the binary mixture with the two-sinker densimeter at our disposal [15]. The measurements were carried out along the isotherm $T = 293.150$ K in the pressure range from 8.03 MPa to 0.51 MPa; the relative expanded combined uncertainty ($k=2$) of the density measurements was 0.015 %. Based on the result of these measurements, the composition of the gas mixture was determined. The result was $x_{\text{O}_2} = 0.2094$ mole fraction oxygen and $x_{\text{N}_2} = 0.7906$ mole fraction nitrogen. The expanded uncertainty ($k=2$) of the composition $U(x_{\text{O}_2})$ was estimated to be 0.0012 mole fraction. Hence, the corresponding molar mass is $M_{\text{mix}} = (28.8482 \pm 0.0048) \text{ g}\cdot\text{mol}^{-1}$. The procedure for determining the composition of the gas mixture is described in detail in the Online Resource in Sect. S3.

To prevent any kind of change of the mixture composition (e.g., due to phase separation), the sample was handled very carefully. Filling the sample into the measuring cell of the densimeter with the correct composition was essential. Hence, the sample cylinder was prepared according to the following procedure: (1) Rolling the sample cylinder for at least 2 h to re-homogenize the gas mixture. (2) Heating the cylinder at the bottom part for at least 3 h using a heating jacket to obtain vortices inside the sample cylinder for homogenizing the gas. (3) Filling the gas mixture into the well-evacuated system to a pressure of about 0.2 MPa through the evacuated filling line and leaving the sample with a residence time of about 2 min before evacuating the apparatus again. Step (3) was repeated three times before the final filling. Thereby, residual gas from previously studied samples is removed to prevent an unwanted compositional change of the new sample.

2.4 Experimental Procedures

The density measurements presented in this work were performed in different states of the studied air-like binary mixture, i.e., in the homogeneous liquid region, the homogeneous gas region, and the supercritical region. All measurements were carried out along isotherms and, depending on the respective state of the fluid, different procedures of filling and operating the apparatus were applied.

2.4.1 Measurements in the Homogeneous Liquid Region

For density measurement of liquefied gases, the details of filling the densimeter and the basic procedure of operating the apparatus were described by Richter *et al.* [3]. We used this procedure for our previous density measurements on six synthetic LNG mixtures, nine methane-rich binary mixtures and two liquefied biogases [3–7]. Here, this established procedure was applied for the density measurements of the liquefied air-like binary mixture at $T = (100, 115, \text{ and } 130)$ K. It is important to mention that our densimeter involves the application of a special VLE-cell, which serves as a buffer for the unavoidable phase transition

(vapor–liquid) between the liquefied sample in the cryogenic measuring cell and the gaseous sample inside the pressure measurement circuit that is kept at a constant temperature of about 313.15 K. The temperatures of the measuring cell and the VLE-cell can be controlled independently of each other at different set points. Since all areas of the measurement system are interconnected, the pressure is everywhere the same (apart from a pressure head correction).

First, we filled the densimeter at ambient temperature to a pressure higher than the cricondenbar pressure (e.g., $p_{fill} \approx 8.0$ MPa for the present measurements); for example, see Fig. 1. Then, the measuring cell and the VLE-cell were cooled simultaneously at constant pressure by continuously adding sample to the system until the VLE-cell had reached a slightly subcritical temperature, or at least a temperature considerably below the temperature at the cricondenbar pressure p_{ccp} . We maintained this temperature of the VLE-cell, while the measuring cell was cooled further to the desired set-point temperature and finally controlled to achieve stable sample conditions. Thereby, the filling procedure was completed, and the first density value was measured at $p > p_{ccp}$. This supercritical filling

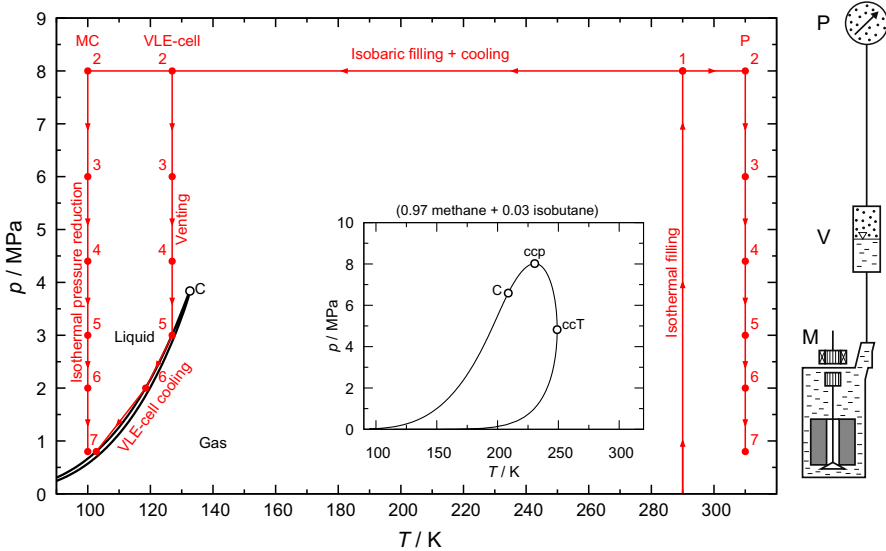


Fig. 1 Left: Principle of the filling and liquefaction procedure shown in a p , T -diagram for the binary mixture (0.2094 oxygen + 0.7906 nitrogen, mole fractions). As an example, the points to be measured at $T = 100$ K are plotted. The phase envelope was calculated using the mixture model of Lemmon *et al.* [8] for the system (nitrogen + argon + oxygen). Right: Schematic presentation of the measurement system consisting of the measuring cell (M), VLE-cell (V), and pressure measurement system (P). The characteristic points are: C, critical point; ccp, cricondenbar; ccT, cricondentherm; $T_C = 132.35$ K, $p_C = 3.7786$ MPa, $\rho_C = 334.8$ kg·m⁻³, $p_{ccp} = 3.7796$ MPa, $T_{ccT} = 132.37$ K; the values were calculated with the mixture model of Lemmon *et al.* [8]. For many binary mixtures, the pressure p_{ccp} is much higher and the temperature difference between the saturated liquid and the saturated vapor line is much larger as in the present case. For example, this is illustrated by the small inserted diagram for a (0.970 methane + 0.030 isobutane) mixture [5]. Here, the phase envelope was calculated using the GERG-2008 equation of state [9, 10]

procedure allows to preserve the composition of the gas mixture inside the sample cylinder for the liquefied sample.

After the first density measurement above p_{ccp} (point 2 in Fig. 1), the pressure was reduced by venting gaseous sample from the system to desired pressures still above p_{ccp} to conduct further measurements in the supercritical region (points 3 and 4 in Fig. 1). For the last (p , T) state point obtained by venting sample from the system, the pressure was below the cricondenbar pressure (point 5 in Fig. 1). This pressure reduction, at an approximately constant temperature of the VLE-cell, results in a vapor–liquid equilibrium forming in the VLE-cell. The venting was stopped, when a liquid volume fraction of about 30 % was established in the VLE-cell (point 5 in Fig. 1); this condition could be detected by a liquid-level indicator (see Online Resource, Sect. S1, Fig. S2). The respective pressure for the set-point temperature of the VLE-cell can be approximately calculated in advance with an adequate mixture model, e.g., the mixture model of Lemmon *et al.* [8], or the GERG-2008 equation of state [9, 10]. At this point, the next density measurement was carried out.

To measure densities at further (p , T) state points in the homogeneous liquid phase, the pressure in the system was no longer adjusted by venting sample from the system, but via reducing the temperature of the VLE-cell. Hence, from this point on, the total mass of fluid in the system remained constant, i.e., it is approximately an isochoric system. By reducing the temperature of the VLE-cell, the pressure in the entire system is decreased accordingly for further density measurements in the homogeneous liquid region (points 6 and 7 in Fig. 1). The last point 7 was always measured just above the calculated saturated liquid pressure. The respective VLE-cell temperature for a desired pressure was approximately determined via mass balance calculations using the GERG-2008 equation [9, 10]. The determined temperature for the desired pressure was always slightly above the respective saturated liquid temperature of the binary mixture, resulting in a liquid volume fraction inside the VLE-cell between 30 % and 70 %. For each investigated isotherm, we filled the densimeter separately.

For the pressure measurement in the homogeneous liquid region at $T=(100, 115, \text{ and } 130)$ K, we used three pressure transmitters; it is described in detail in a previous paper by Richter *et al.* [3]. The transmitters cover the pressure ranges from 0 MPa to 0.69 MPa, 0 MPa to 3.45 MPa, and 0 MPa to 13.8 MPa; their expanded uncertainty ($k=1.73$) in pressure is $U(p)=0.01 \% \cdot p_{\text{max}}$. We used the transmitters up to approximately $0.8 \cdot p_{\text{max}}$, i.e., >0.18 MPa to ≤ 0.50 MPa; >0.50 MPa to ≤ 2.7 MPa, and >2.7 MPa to ≤ 10.8 MPa, respectively. According to our experience, the transmitters show then a better long-term stability of the calibration curve.

2.4.2 Measurements in the Homogeneous Gas Region and the Supercritical Region

For the density measurements along the three supercritical isotherms $T=(145, 220, \text{ and } 298.15)$ K, the filling procedure was almost the same as described above for the density measurements of the liquefied air-like mixture at $T=(100, 115, \text{ and } 130)$ K. At first, the densimeter was filled at ambient temperature to a pressure of $p_{\text{fill}} \approx 8.0$ MPa (see Fig. 1). Then, the measuring cell and the VLE-cell were cooled simultaneously at constant pressure by continuously adding sample

to the system until the VLE-cell had reached a temperature of, e.g., about 20 K higher than the desired temperature of the measuring cell of, e.g., $T = 145$ K. We maintained this temperature of the VLE-cell at a constant value, while the measuring cell was cooled further to the desired temperature where it was controlled to maintain a constant value. Thereby, the filling procedure was completed, and the first density value at $p \approx 8.0$ MPa was measured. To measure the densities at all further desired (p, T) state points, the pressure was reduced each time by venting gas from the system to the next target pressure. The last point was at $p \approx (1.0$ or $0.5)$ MPa.

For the density measurements in the homogeneous gas region along the three isotherms $T = (100, 115, \text{ and } 130)$ K, the filling procedure was the same as described above for the density measurements at supercritical temperatures. However, we only filled the system to a pressure about (0.03 to 0.3) MPa below the saturated vapor pressure (please note: this filling procedure for gas densities is not shown separately in Fig. 1). Then, the cooling procedure and the measurements were carried out in the same way as described above for the density measurements on the supercritical isotherms. The temperature of the VLE-cell was set to a value which was about 20 K higher than the desired temperature of the measuring cell. The first density was measured at a pressure about (0.03 to 0.3) MPa below the saturated vapor pressure, and the last point was measured at $p \approx (0.2, 0.3, \text{ or } 0.5)$ MPa.

Up to now, our low-temperature single sinker densimeter was only used for density measurements of cryogenic liquids with relatively high densities [3–7]. In the present work, however, also measurements of low gas densities were carried out as described above. To accurately measure the pressure of the gas, we used a piston gauge (Fluke, PG-7601-CE); its expanded uncertainty ($k = 1.73$) is (0.0035 % $p + 20$ Pa). An integrated barometer was used to determine the ambient air pressure; its expanded uncertainty ($k = 1.73$) is 140 Pa. The temperature measurement and its expanded uncertainty ($k = 1.73$) of 0.015 K were already described in detail by Richter *et al.* [3]. Furthermore, the relative expanded uncertainty ($k = 2$) in density measurement was also discussed there in detail, and it was given to be 0.0080 % for liquid densities. In the present work, however, we also measured low gas densities. Therefore, we evaluated the expanded uncertainty ($k = 2$) for these measurements with $0.0030 \text{ kg}\cdot\text{m}^{-3}$, as the minimum uncertainty, which corresponds to 0.30 %/ $(\rho/\text{kg}\cdot\text{m}^{-3})$. This uncertainty is mainly caused by the analytical balance used (readability: 0.01 mg); see Richter *et al.* [3] and Figs. S1 and S2 in the Online Resource in Sect. S1. Hence, for all (p, ρ, T) state points investigated, the uncertainty of the density measurement is $0.0030 \text{ kg}\cdot\text{m}^{-3}$ or 0.0080 %, whichever is greater.

2.5 Uncertainty in Density Measurements

The combined uncertainty in density measurement was determined in line with the GUM [16] (ISO/IEC Guide). With the assumption that there is no correlation of the input quantities, the expanded combined uncertainty U for the determination of cryogenic liquid densities using the above described densimeter can be determined by

$$U(\rho) = k \cdot u_c(\rho(T, p, x)) = k \cdot \left[u(\rho)^2 + \left(\left(\frac{\partial \rho}{\partial p} \right)_T \cdot u(p) \right)^2 + \left(\left(\frac{\partial \rho}{\partial T} \right)_p \cdot u(T) \right)^2 + u(\rho(x))^2 + u(\rho_{\text{repro}})^2 + u(\rho_{\text{corr}})^2 \right]^{1/2}, \quad (8)$$

where $u(\rho)$, $u(T)$, and $u(p)$ are the standard uncertainties in density, temperature, and pressure, respectively; $u(\rho(x))$ corresponds to the standard uncertainty in the density resulting from the uncertainty of the gas composition; $u(\rho_{\text{repro}})$ accounts for an additional uncertainty from the reproducibility of our measurements; and $u(\rho_{\text{corr}})$ takes into account the uncertainty of the correction of the force transmission error. A detailed description of the uncertainty evaluation was reported in previous works [3–5]. The expanded combined uncertainty in measurement was evaluated for each measured state point. The main contributions to the combined uncertainty are due to the pressure measurement (up to 63 %), the correction of the FTE (up to 60 %), and the uncertainty of the gas composition (up to 76 %); the respective contribution depends on the respective (p , ρ , T) state point. As a typical example, Table 1 shows the various contributions to the relative combined expanded uncertainty in density for the state point at $T = 115.000$ K, $p = 2.47663$ MPa, and $\rho = 672.741$ kg·m⁻³.

3 Results and Discussion

Densities of an air-like binary mixture (0.2094 oxygen + 0.7906 nitrogen, mole fractions) were measured along six isotherms in the homogeneous gas, the homogeneous liquid, and in the supercritical region. The measurements were carried out at

Table 1 Uncertainty budget for the density measurements. As an example, the uncertainty was calculated for the binary mixture (0.2094 oxygen + 0.7906 nitrogen, mole fractions) at $T = 115.000$ K, $p = 2.47663$ MPa, and $\rho_{\text{exp}} = 672.741$ kg·m⁻³ (see Table 2)

Source of uncertainty	Expanded uncertainty ($k = 2$ or 1.73)	Distribution	Standard uncertainty in density (%)
Density measurement ^a	0.0080 %	Normal	0.0040
Pressure measurement ^a	345 Pa	Rectangular	0.0003
Temperature measurement ^a	15 mK	Rectangular	0.0106
Composition of the gas mixture ^b	0.12 mol%	Normal	0.0359
Reproducibility of the measurements ^c	0.0100 %	Normal	0.0050
Density correction ^d	0.0552 %	Normal	0.0276
Relative expanded combined uncertainty in density ($k = 2$): $U(\rho) = 0.094$ %			

^aThe uncertainties in density, pressure, and temperature measurement are given in Sect. 2.4

^bThe uncertainty of the composition of the gas mixture is given in Sect. 2.3

^cThe uncertainty of the reproducibility of the measurements has been discussed in a previous paper of our group by Richter *et al.* [3] in 2016

^dCorrection of the measured densities due to the force transmission error (FTE), see Sect. 2.2

$T=(100, 115, 130, 145, 220, \text{ and } 298.15)$ K at pressures up to 8.0 MPa; the critical temperature of the binary mixture is $T_C=132.35$ K (as calculated with the mixture model of Lemmon *et al.* [8]). Furthermore, saturated liquid and saturated vapor densities were determined at $T=(100, 115, \text{ and } 130)$ K. Figure 2 shows an overview of the measured state points in a p, ρ -diagram.

3.1 Results for Homogeneous Gas, Liquid, and Supercritical Densities

Density measurements in the homogeneous liquid phase at $T=(100, 115, \text{ and } 130)$ K started at the supercritical filling pressure of $p \approx 8.0$ MPa. To avoid vaporization of the mixture in the measuring cell, the measurements were terminated at pressures at least 0.1 MPa above the saturated liquid pressure as calculated with the mixture model of Lemmon *et al.* [8] for the system (nitrogen + argon + oxygen). Two or three replicates were taken at each (p, ρ, T) state point. Density measurements in the homogeneous gas phase at $T=(100, 115, \text{ and } 130)$ K started from 0.03 MPa to 0.3 MPa below the saturated vapor pressure and ended at the lowest pressure of (0.2, 0.3, and 0.5) MPa, respectively. The density measurements in the supercritical region at $T=(145, 220, \text{ and } 298.15)$ K started at $p \approx 8.0$ MPa and were completed at (0.5 or 1.0) MPa.

Our experimental results are listed in Table 2 together with their uncertainties as discussed in Sects. 2.4.2 and 2.5. The relative expanded combined uncertainty ($k=2$) in density was estimated to be between 0.03 % and 0.13 %, except for four values near the critical point, where the uncertainty gets as large as 0.24 %.

In Figs. 3, 4, 5, the relative deviations of the experimental densities from values calculated with the mixture model of Lemmon *et al.* [8] for the system (nitrogen + argon + oxygen) are plotted versus pressure; the numerical values of these deviations are listed in Table 2. For comparison, values calculated with the well-established GERG-2008 equation of state of Kunz and Wagner [9, 10] (as implemented in the TREND 5.0 software package [17]) are also plotted in the figures; the deviations of the experimental values from values calculated with this equation are also listed in Table 2. The GERG-2008 equation describes the thermodynamic properties of fluid mixtures for up to 21 components relevant to natural gas and similar mixtures, which does not include a binary-specific or generalized departure function for the (nitrogen + oxygen) system but only an adjusted reducing function [9, 10]. Furthermore, the experimental results of five different author groups, listed in Table 3, are plotted in Figs. 3, 4, 5 for comparison. Experimental results of further authors were not considered here because they would overcrowd the figures and not yield any significant contribution.

The authors of the mixture model of Lemmon *et al.* [8] for the system (nitrogen + argon + oxygen) report an estimated uncertainty of 0.1 % for the densities calculated with this mixture model. Hence, the mixture model describes almost all of our new experimental data in the homogeneous gas and liquid region within this small uncertainty. Only five values of the homogeneous regions deviate by up to -0.133 %, e.g., see Fig. 5 at $T=145$ K and Table 2. However, in the gas region for the low gas densities at $T=(100, 115, 130, \text{ and } 145)$ K, our measurements and

Table 2 Experimental densities^{a,b} ρ_{exp} for the binary mixture (0.2094 oxygen + 0.7906 nitrogen, mole fractions) and their relative deviations from densities ρ_{calc} and ρ_{GERG} calculated with the mixture model of Lemmon *et al.* [8] for the system (nitrogen + argon + oxygen) and the GERG-2008 equation of state [9, 10], respectively, where p is the pressure, T is the temperature (ITS-90), and $100(U(\rho)/\rho)$ is the relative expanded combined uncertainty ($k=2$)

p/MPa	$\rho_{\text{exp}}/(\text{kg}\cdot\text{m}^{-3})$	$100(U(\rho)/\rho)$	$100(\rho_{\text{exp}}-\rho_{\text{calc}})/\rho_{\text{calc}}$	$100(\rho_{\text{exp}}-\rho_{\text{GERG}})/\rho_{\text{GERG}}$
$T=100.000\text{ K}^c$				
7.94990	794.290	0.087	-0.026	-0.269
6.03763	787.036	0.087	-0.025	-0.269
4.42306	780.425	0.088	-0.026	-0.275
3.00703	774.201	0.089	-0.028	-0.282
1.97577	769.367	0.089	-0.030	-0.288
0.97649	764.402	0.090	-0.032	-0.295
0.77693	763.372	0.090	-0.033	-0.302
0.66706	762.802 ^d	0.090	-0.033	-0.304
0.56956	22.736 ^d	1.179	-0.040	-0.177
0.50010	19.553	0.069	-0.034	0.017
0.29986	11.118	0.084	-0.018	0.009
0.19976	7.235	0.109	0.003	0.019
$T=115.000\text{ K}^c$				
7.98396	716.907	0.084	0.013	-0.220
6.05431	704.052	0.086	0.008	-0.236
4.63125	693.095	0.088	0.003	-0.255
3.03319	678.578	0.092	-0.006	-0.287
2.47663	672.741	0.094	-0.011	-0.304
1.87238	665.781	0.097	-0.016	-0.326
1.66855	663.259 ^d	0.102	-0.018	-0.337
1.52582	62.627 ^d	1.525	-0.105	-0.315
1.50057	61.071	0.067	-0.102	0.119
1.00032	35.688	0.057	-0.061	0.049
0.80063	27.432	0.057	-0.046	0.031
0.50047	16.261	0.063	-0.028	0.009
0.30032	9.458	0.081	0.004	0.022
$T=130.000\text{ K}^c$				
8.00539	618.704	0.090	0.029	-0.168
6.00401	587.228	0.102	0.024	-0.214
4.50381	548.460	0.132	0.010	-0.303
4.00344	526.796	0.164	-0.012	-0.377
3.60314	498.154	0.243	-0.079	-0.569
3.44155	476.527 ^d	1.377	-0.119	-1.194
3.33149	185.777 ^d	4.855	-0.165	0.231
3.00106	134.915	0.109	-0.143	0.453
2.50077	95.756	0.068	-0.108	0.196
2.00030	68.879	0.056	-0.080	0.106

Table 2 (continued)

p/MPa	$\rho_{\text{exp}}/(\text{kg}\cdot\text{m}^{-3})$	$100(U(\rho)/\rho)$	$100(\rho_{\text{exp}}-\rho_{\text{calc}})/\rho_{\text{calc}}$	$100(\rho_{\text{exp}}-\rho_{\text{GERG}})/\rho_{\text{GERG}}$
1.49993	47.611	0.051	-0.057	0.055
0.99981	29.688	0.050	-0.035	0.024
0.49946	14.011	0.060	-0.010	0.011
$T=145.000\text{ K}^c$				
8.00475	472.453	0.118	0.025	-0.044
7.00375	423.759	0.148	0.003	0.089
6.00300	337.914	0.191	-0.057	0.472
5.00265	223.159	0.128	-0.116	0.517
4.00211	145.063	0.073	-0.133	0.193
3.00146	94.073	0.054	-0.100	0.082
2.00034	56.200	0.046	-0.065	0.030
0.99969	25.733	0.046	-0.031	0.004
0.49932	12.375	0.058	-0.004	0.010
$T=220.000\text{ K}^c$				
8.00371	141.036	0.039	-0.046	0.062
6.00277	103.475	0.036	-0.041	0.040
4.00147	67.148	0.034	-0.030	0.019
2.00030	32.570	0.033	-0.018	0.000
1.00022	16.031	0.039	-0.010	-0.003
0.49975	7.945	0.059	-0.009	-0.007
$T=298.150\text{ K}^c$				
8.00440	94.072	0.030	-0.027	0.025
6.00351	70.578	0.029	-0.022	0.013
4.00242	46.977	0.029	-0.016	0.003
2.00119	23.408	0.030	-0.008	-0.002
1.00050	11.675	0.040	-0.003	-0.001

The measurements were carried out in the homogeneous gas phase and liquid phase as well as in the supercritical region

^aAn electronically readable table of the density measurements is given in the Online Resource in Sect. S4

^bThe expanded uncertainty ($k = 1.73$) in temperature measurement is $U(T) = 0.015\text{ K}$. The expanded uncertainty in pressure and density measurement is given in Sect. 2.4

^cThe measured temperatures were rounded to the even target temperatures. Accordingly, the experimental densities were corrected using the sensitivity of density to temperature $(\delta\rho_{\text{calc}}/\delta T)_p$, calculated with the mixture model of Lemmon *et al.* [8]. For temperature corrections of less than 52 mK, the uncertainty of density correction due to the uncertainty of the equation of state can be neglected in the uncertainty budget of the relative expanded combined experimental uncertainty ($k = 2$) in density

^dSaturated liquid and saturated vapor densities determined by extrapolation; see Sect. 3.2 and Table 4

also the results of three other authors (Blanke [21], Michels *et al.* [18], and Howley *et al.* [22]) show increasing negative deviations from the zero line with increasing pressure (see Figs. 4 and 5). These systematic deviations suggest that the cross second virial coefficient of the mixture model is probably not optimal to describe

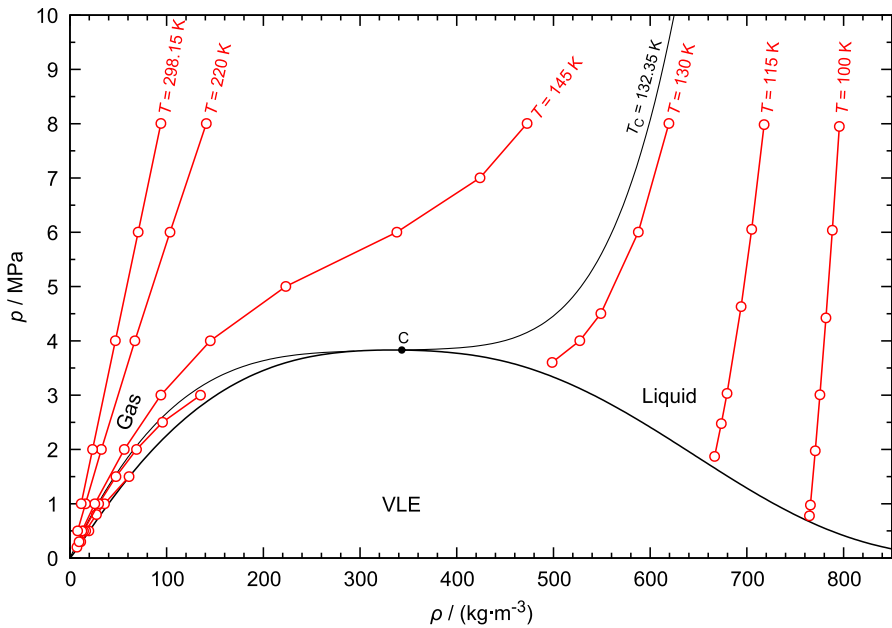


Fig. 2 p , ρ -diagram of the binary mixture (0.2094 oxygen + 0.7906 nitrogen, mole fractions). The phase boundary and the isotherms were calculated with the mixture model of Lemmon *et al.* [8] for the system (nitrogen + argon + oxygen); \circ , (p , ρ , T) state points measured in the present work; \bullet , critical point ($T_{\text{crit}} = 132.35$ K, $p_{\text{crit}} = 3.7786$ MPa, $\rho_{\text{crit}} = 334.8$ kg·m $^{-3}$).

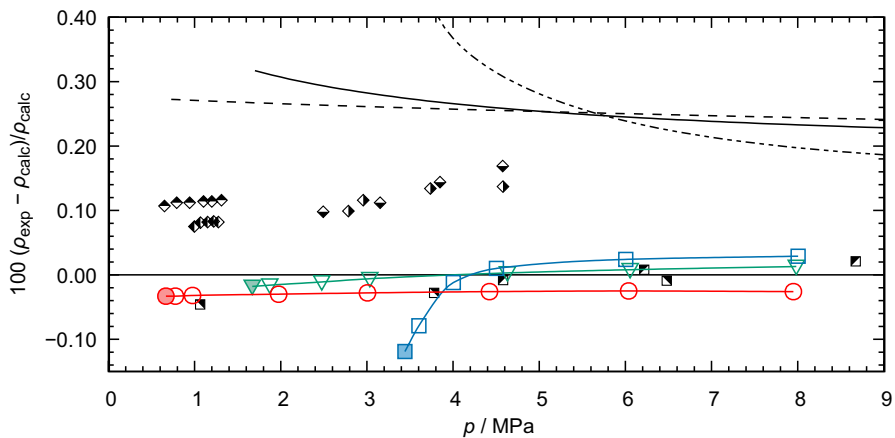


Fig. 3 Relative deviations of experimental and calculated densities ρ in the homogeneous liquid region for the (0.2904 oxygen + 0.7906 nitrogen, mole fractions) mixture from densities ρ_{calc} calculated with the mixture model of Lemmon *et al.* [8] for the system (nitrogen + argon + oxygen) (zero line). Densities measured in the present work: \circ , $T = 100$ K; ∇ , $T = 115$ K; \square , $T = 130$ K. Saturated liquid densities, determined by extrapolation, are marked with filled symbols; see Sect. 3.2 and Table 4. Densities calculated with the GERG-2008 equation of state [9, 10]: ---, $T = 100$ K; - · - ·, $T = 115$ K; - · · ·, $T = 130$ K. Measurements of other authors are plotted for comparison: Blanke [21]: \blacklozenge , $T \approx 98$ K; \blacklozenge , $T \approx 106$ K; \blacklozenge , $T \approx (116 \text{ to } 119)$ K; \blacklozenge , $T \approx (123 \text{ to } 126)$ K; Howley *et al.* [22]: \blacksquare , $T \approx (92 \text{ to } 96)$ K; \blacksquare , $T \approx (115 \text{ to } 120)$ K

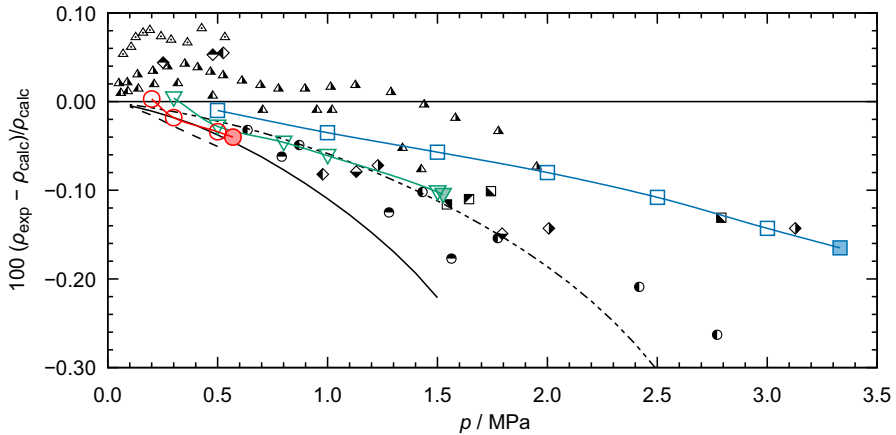


Fig. 4 Relative deviations of experimental and calculated densities ρ in the homogeneous gas region (for $T < T_C$) for the (0.2904 oxygen+0.7906 nitrogen, mole fractions) mixture from densities ρ_{calc} calculated with the mixture model of Lemmon *et al.* [8] for the system (nitrogen + argon + oxygen) (zero line). Densities measured in the present work: \circ , $T=100$ K; ∇ , $T=115$ K; \square , $T=130$ K; Saturated vapor densities, determined by extrapolation, are marked with filled symbols; see Sect. 3.2 and Table 4 below. Densities calculated with the GERG-2008 equation of state [9, 10]: ---, $T=100$ K; - · -, $T=115$ K; · · ·, $T=130$ K. Measurements of other authors are plotted for comparison: Romberg [20]: \triangle , $T=103.240$ K; \blacktriangle , $T=117.123$ K; \blacktriangle , $T=122.223$ K; Blanke [21]: \blacklozenge , $T \approx 100$ K; \blacklozenge , $T \approx (108 \text{ to } 110)$ K; \blacklozenge , $T \approx 122$ K; \blacklozenge , $T \approx 130$ K; Michels *et al.* [18]: \bullet , $T=118.15$ K; \bullet , $T=128.15$ K; Howley *et al.* [22]: \blacksquare , $T=120$ K; \blacksquare , $T=125$ K; \blacksquare , $T=130$ K

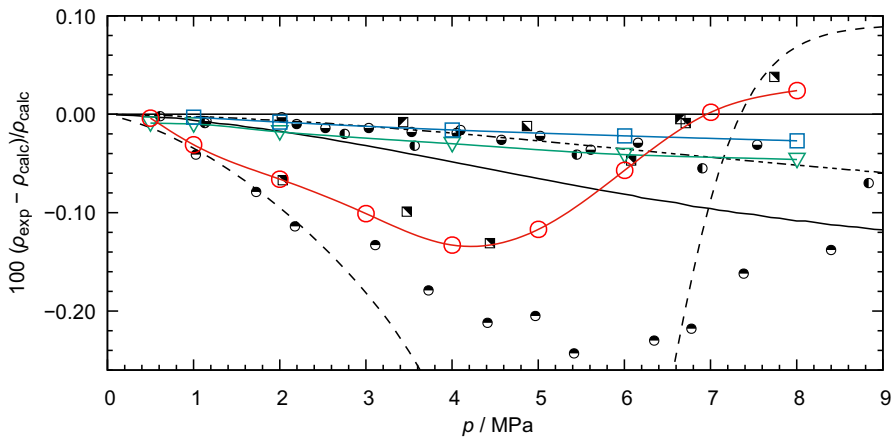


Fig. 5 Relative deviations of experimental and calculated densities ρ in the supercritical region ($T_C = 132.35$ K) for the (0.7906 nitrogen+0.2904 oxygen, mole fractions) mixture from densities ρ_{calc} calculated with the mixture model of Lemmon *et al.* [8] for the system (nitrogen + argon + oxygen) (zero line). Densities measured in the present work: \circ , $T=145$ K; ∇ , $T=220$ K; \square , $T=298.15$ K. Densities calculated with the GERG-2008 equation of state [9, 10]: ---, $T=145$ K; - · -, $T=220$ K; · · ·, $T=298.15$ K. Measurements of other authors are plotted for comparison: Michels *et al.* [18]: \bullet , $T=148.15$ K; \bullet , $T=223.15$ K; \bullet , $T=298.15$ K; Howley *et al.* [22]: \blacksquare , $T \approx 145$ K; \blacksquare , $T \approx 220$ K; \blacksquare , $T \approx 300$ K

Table 3 Review of selected density measurements on air of five different authors^a

Author	Year	No. of points	T/K	p/MPa	$\rho/(\text{kg}\cdot\text{m}^{-3})$	Composition
Michels <i>et al.</i> [18]	1954	117	273–348	0.7–78.6	8–525	Air ^b
Michels <i>et al.</i> [19]	1954	221	118–248	0.6–102.3	9–723	Air ^b
Romberg [20]	1971	114	84–122	0.0–2.0	1–82	Air ^b
Blanke [21] ^c	1973	403	53–170	0.0–4.9	1–954	Air ^b
Howley <i>et al.</i> [22]	1994	286	67–400	1.1–35.2	57–933	Air ^b

^aFurther authors who measured the density on air or air-like mixture (0.21 oxygen + 0.79 nitrogen) are listed in Lemmon *et al.* [8] and Kunz and Wagner [23]

^bComposition of the air mixtures (nitrogen + oxygen + argon), respectively, in mole fractions: Blanke: 0.7841, 0.2066, 0.0093; Howley (two samples): 0.78122, 0.20966, 0.00922, and 0.78120, 0.20958, 0.00922; Michels *et al.*: not given; Romberg: 0.7816, 0.2091, 0.0093; Lemmon *et al.* [8]: 0.7812, 0.2096, 0.0092 (composition used for the equation of state for air)

^cA summary of the Ph.D. thesis of Blanke [21] was also published in a paper by Blanke [24] in 1976

the experimental results. The selected experimental results of the five author groups listed in Table 3 were evaluated by Lemmon *et al.* [8] for the development of the multi-parameter mixture model and used to fit the coefficients within the model. The deviations of these experimental results from the model are less than 0.2 % in most cases, see Figs. 3, 4, 5. The GERG-2008 equation of state [9, 10] also describes our new measurement results within the reported uncertainty for this equation. However, the given uncertainties are (0.5 to 1.0) % for the liquid phase and (0.3 to 1.0) % for the gas phase, which is much larger than for the mixture model of Lemmon *et al.* with 0.1 %. Relatively large deviations occur between densities calculated with the GERG-2008 equation and our experimental densities in the homogeneous liquid region at $T=(100, 115, \text{ and } 130)$ K, namely, between about 0.17 % and 0.38 % (except for one value at 0.57 %); see Fig. 3 and Table 2. Moreover, in the supercritical region at $T=145$ K deviations of up to about 0.5 % occur; see Fig. 5 and Table 2. However, it should be mentioned here that the GERG-2008 equation was developed with the focus on natural gases, and our binary mixture (oxygen+nitrogen) is not described by a binary-specific or generalized departure function. Finally, it is worth to mention that our new experimental data and the results of Howley *et al.* [22] at $T \approx 145$ K agree within 0.02 % (see Fig. 4), and they also agree very well in the liquid phase (see Fig. 3).

3.2 Determination of Saturated Liquid and Saturated Vapor Densities

The saturated liquid and saturated vapor densities at $T=(100, 115, \text{ and } 130)$ K were determined by extrapolating the experimental results along the isotherms in the homogeneous liquid and vapor regions to the saturated liquid and saturated vapor pressure of the mixture, respectively. For this purpose, the relative deviations of the experimental densities, ρ_{exp} , from densities, ρ_{calc} , calculated with the mixture model of Lemmon *et al.* [8] were extrapolated to the saturation pressures, see also Figs. 3 and 4. The saturated liquid and saturated vapor pressures needed for these

extrapolations were calculated with the mixture model of Lemmon *et al.* [8]; the uncertainty was reported by the authors to be generally within 1 %. The influence of the extrapolation on the uncertainty of the results is relatively large for the saturated vapor densities and the saturated liquid density at $T=130$ K, which is due to the large isothermal compressibility $(\partial\rho/\partial p)_T$ in combination with the uncertainty of the vapor pressure of 1 % [8]. The results are listed in Table 4 including their uncertainties.

The relative deviations of the determined saturated liquid and saturated vapor densities of our binary mixture (0.2094 oxygen+0.7906 nitrogen, mole fractions) from values, ρ_{calc} , calculated with the mixture model of Lemmon *et al.* [8] are plotted in Fig. 6; the numerical values of the relative deviations are listed in Table 4. Moreover, the saturation densities are also presented in the previously shown Figs. 4 and 5.

The uncertainty of the saturated liquid and saturated vapor densities calculated with the mixture model of Lemmon *et al.* [8] was estimated by the authors to be 0.1 %. Hence, the mixture model describes our new saturation densities clearly within their uncertainties; see Table 4. For comparison, saturated densities calculated with the GERG-2008 equation of state of Kunz and Wagner [9, 10] (as implemented in the TREND 5.0 software package [17]) are also plotted in the figure; the deviations of the saturated densities determined in the present work from values

Table 4 Saturated liquid and saturated vapor densities^{a,b} $\rho_{sat,exp}$ for the binary mixture (0.2094 oxygen+0.7906 nitrogen, mole fractions) and their relative deviations from densities $\rho_{sat,calc}$ and $\rho_{sat,GERG}$ calculated with the mixture model of Lemmon *et al.* [8] for the system (nitrogen + argon + oxygen) and the GERG-2008 equation of state of Kunz and Wagner [9, 10], respectively, where p_{sat} is the respective saturation pressure^c, T is the temperature (ITS-90), and $100(U(\rho)/\rho)$ is the relative expanded combined uncertainty ($k=2$)

T/K	p_{sat}/MPa^b	$\rho_{sat,exp}/(kg\cdot m^{-3})$	$100(U(\rho)/\rho)$	$100(\rho_{sat,exp}-\rho_{sat,calc})/\rho_{sat,calc}$	$100(\rho_{sat,exp}-\rho_{sat,GERG})/\rho_{sat,GERG}$
Saturated vapor densities					
100.000	0.56956	22.736	1.179 ^c	-0.040	-0.177
115.000	1.52582	62.627	1.525 ^c	-0.105	-0.315
130.000	3.33149	185.777	4.855 ^c	-0.165	0.231
Saturated liquid densities					
100.000	0.66706	762.802	0.090	-0.033	-0.304
115.000	1.66855	663.259	0.102	-0.018	-0.337
130.000	3.44155	476.527	1.377 ^c	-0.119	-1.194

^aAn electronically readable table of the density measurements is given in the Online Resource in Sect. S4

^bThe saturated liquid and saturated vapor densities were determined by extrapolating the experimental densities along the isotherms in the homogeneous liquid and vapor region to the saturated liquid and saturated vapor pressure, respectively. The vapor pressures, p_{sat} , for the binary mixture (0.2094 oxygen + 0.7906 nitrogen, mole fractions) were calculated with the mixture model of Lemmon *et al.* [8]; their uncertainty was reported to be generally within 1 %

^cThe large uncertainty of this value is due to the large isothermal compressibility $(\partial\rho/\partial p)_T$ in combination with the uncertainty of the vapor pressure of 1 % [8]

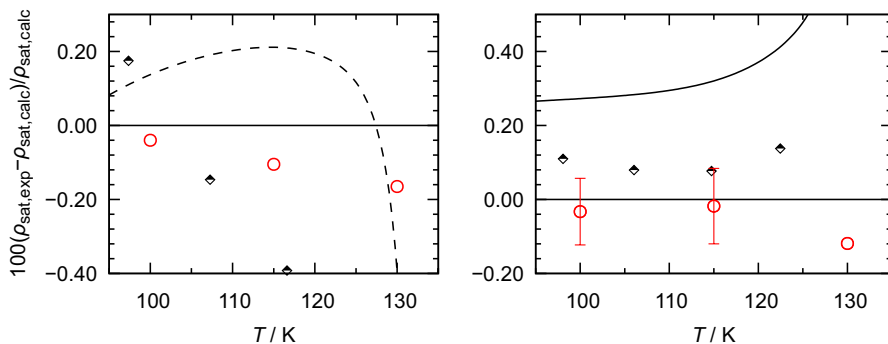


Fig. 6 Relative deviations of experimentally ascertained saturated vapor densities (left figure) and saturated liquid densities (right figure), $\rho_{\text{sat,exp}}$, for the (0.7906 nitrogen + 0.2904 oxygen, mole fractions) mixture from densities, $\rho_{\text{sat,calc}}$, calculated with the mixture model of Lemmon *et al.* [8] for the system (nitrogen + argon + oxygen) (zero line). \circ , densities determined in the present work. The uncertainties of our new saturated density data are illustrated partially with error bars; for all uncertainties see Table 3. Densities calculated with the GERG-2008 equation of state [9, 10]: - - -, saturated vapor densities; - - -, saturated liquid densities. Experimental results of other authors are plotted for comparison: \blacklozenge , Blanke [21] saturated vapor and saturated liquid densities

calculated with this equation are also listed in Table 4. Moreover, the experimental results of Blanke [21] are plotted in Fig. 6 for comparison. The saturated densities reported by Michels *et al.* [18] are not shown because they deviate from the zero line between 1 % and 4 % in most cases.

3.3 Verification of the Apparatus-specific constant ϵ_p

The re-determination of the apparatus-specific constant of our densimeter, $\epsilon_p = (53 \pm 2) \times 10^{-6}$, was already briefly explained in Sect. 2.2.3, and it was stated that it is not temperature dependent [1, 2]. This is also shown and discussed here. In Figs. 4 and 5, it can be observed that our density measurements along six isotherms in the low-density gas region can be extrapolated to the zero density at $p=0$. The deviations of the extrapolated values from the zero line at $T=(100, 115, 130, 145, 220, \text{ and } 298.15)$ K are less than ± 0.02 %. The low experimental densities on these isotherms were corrected by the fluid-specific effect which is up to $\epsilon_{\text{fse}} = -(11222, 9752, 8621, 7724, 5073, \text{ and } 3730) \times 10^{-6}$, respectively (see Online Resource, Sect. S2.4); the expanded uncertainty ($k=2$) of the correction model, represented by the term ϵ_{fse} in Eq. 7, was estimated to be 4 %, which corresponds to $(449, 390, 345, 309, 203, \text{ and } 149) \times 10^{-6}$, respectively. Hence, as already mentioned in Sect. 2.2.3, these results confirm the reliability of the apparatus-specific constant $\epsilon_p = (53 \pm 2) \times 10^{-6}$ as a constant that is valid for the entire temperature range from 100 K to 300 K. Since the susceptibility of oxygen in our air-like binary mixture (0.2094 mol fraction oxygen in nitrogen) is very large, this mixture was very suitable for checking our apparatus-specific constant and the correction model. As a final remark, we would like to mention that we assume that the last (p, ρ, T) state point

on each of the four isotherms at $T=(100, 115, 130, \text{ and } 145)$ K and $p \approx (0.20, 0.30, 0.50, \text{ and } 0.50)$ MPa, respectively, could have been slightly influenced by sorption effects. This means that a fraction of the lower boiling gas, in our case oxygen, was adsorbed on the inner surfaces of the measuring cell at high pressures and then, at low pressures, it desorbed. As a result of this desorption, the density of the gas in the measuring cell could increase slightly since the density of the component oxygen is greater than that of nitrogen. This behavior of gas mixtures has already been described in previous works [25–29]. Therefore, these last state points on each of the four isotherms should not be taken into account when extrapolating the measurements to the density $\rho=0$.

In this context it should be mentioned that the density of air was also measured by McLinden in 2006 (unpublished data, see reference 10 in [1]) with the two-sinker densimeter at NIST [30]. A temperature range from 250 K to 460 K was covered at densities up to about $440 \text{ kg}\cdot\text{m}^{-3}$; it was briefly described by McLinden *et al.* in 2007 [1]. Since this two-sinker densimeter (with sinkers made of titanium and tantalum and masses of $m \approx 60$ g) can also be used in the single-sinker mode, the apparatus-specific constant, ε_ρ , could be determined. The result for the NIST densimeter was $\varepsilon_\rho = 51.7 \times 10^{-6}$, which was also valid for the entire temperature range, as in our current case. The comparison of the two apparatus-specific constants shows a mentionable similarity: the two constants agree within 2×10^{-6} , although the designs of the two densimeters are quite different.

Finally, it should be mentioned here that a two-sinker densimeter is more suitable for density measurements on fluids with large magnetic susceptibilities, because it employs a differential method, and the fluid-specific effect, ε_{fse} , is very small since the term ρ_S/ρ_0 in Eq. 7 does not exist for this density measurement method; see also Online Resource, Sect. S3.

4 Conclusion

Accurate density measurements of the air-like binary mixture (0.2094 mol fraction oxygen in nitrogen) were carried out along the six isotherms $T=(100, 115, 130, 145, 220, \text{ and } 298.15)$ K at pressures up to 8.0 MPa. For this study, we used the single-sinker densimeter of our group which was originally developed for density measurements of cryogenic liquid mixtures. Nevertheless, we used this densimeter to measure densities in the homogeneous gas and liquid regions as well as the supercritical region; in total of 52 state points were measured, and six saturation densities were determined. The combined uncertainty ($k=2$) in density is 0.03 % to 0.13 % in most cases. A main contribution to the uncertainty is due to the correction of the force transmission error (FTE). This FTE is caused by the magnetic suspension coupling in our densimeter in combination with the magnetic properties of the fluids under investigation. For paramagnetic fluids (e.g., methane and nitrogen), the FTE is less than 0.018 %, but the component oxygen in our air-like binary mixture is strongly paramagnetic. For this reason, the influence of the FTE on our density measurements was relatively large, namely (0.36 to 1.1) %. Moreover, the magnetic properties of oxygen depend on its density and, therefore, the partial density of oxygen

significantly influences the magnetic properties of our binary mixture. For example, this effect is negligible for low gas densities but it is up to 0.18 % at $T=100$ K and $\rho_{\text{fluid}} \approx 794 \text{ kg m}^{-3}$. To correct this FTE, we use a correction model with an uncertainty of only 4 %. The uncertainty of this model was thoroughly evaluated in Sect. 3.3.

The new experimental results were compared with the mixture model of Lemmon *et al.* [8] for the system (nitrogen + argon + oxygen); see Figs. 3, 4, 5. The relative deviations of our values from densities calculated with this mixture model are less than 0.10 %, except for five values which deviate by up to -0.14 %. Hence, the mixture model is able to describe the new experimental densities of our binary mixture within the reported small uncertainty of only 0.1 %. For comparison, densities calculated with the well-established GERG-2008 equation of state [9, 10] are also plotted in Figs. 3, 4, and 5. Values calculated with this equation deviate from our measurements between about 0.17 % and 0.38 % for the liquid densities at $T=(100, 115, \text{ and } 130)$ K. Since this equation was developed with the focus on natural gases and not for the system (oxygen + nitrogen), the reported uncertainties for this system are (0.3 to 1.0) %; these limits also cover our experimental results. Finally, the experimental results of five other authors are also plotted in Figs. 3, 4, and 5 for comparison with our new measurements; the agreement with our results is better than 0.2 %.

Supplementary Information The online version contains supplementary material available at <https://doi.org/10.1007/s10765-021-02871-4>.

Acknowledgments The authors thank Dr.-Ing. Mohamed A. Ben Souissi of our group for performing density measurements of our air-like binary mixture with the two-sinker densimeter of our group; these measurements at $T = 293.15$ K were the basis for the determination of the composition of our binary mixture. Furthermore, they thank Dr.-Ing. Monika Thol of our institute for helpful discussions regarding the present topic. Moreover, they are thankful to Dr. Eric Lemmon of NIST for providing us with a software for calculations with the mixture model for the system (nitrogen + argon + oxygen).

Funding Open Access funding enabled and organized by Projekt DEAL.

Open Access This article is licensed under a Creative Commons Attribution 4.0 International License, which permits use, sharing, adaptation, distribution and reproduction in any medium or format, as long as you give appropriate credit to the original author(s) and the source, provide a link to the Creative Commons licence, and indicate if changes were made. The images or other third party material in this article are included in the article's Creative Commons licence, unless indicated otherwise in a credit line to the material. If material is not included in the article's Creative Commons licence and your intended use is not permitted by statutory regulation or exceeds the permitted use, you will need to obtain permission directly from the copyright holder. To view a copy of this licence, visit <http://creativecommons.org/licenses/by/4.0/>.

References

1. M.O. McLinden, R. Kleinrahm, W. Wagner, *Int. J. Thermophys.* (2007). <https://doi.org/10.1007/s10765-007-0176-0>
2. R. Kleinrahm, X. Yang, M.O. McLinden, M. Richter, *Adsorption* (2019). <https://doi.org/10.1007/s10450-019-00071-z>

3. M. Richter, R. Kleinrahm, R. Lentner, R. Span, J. Chem. Thermodyn. (2016). <https://doi.org/10.1016/j.jct.2015.09.034>
4. R. Lentner, M. Richter, R. Kleinrahm, R. Span, J. Chem. Thermodyn. (2017). <https://doi.org/10.1016/j.jct.2017.04.002>
5. R. Lentner, P. Eckmann, R. Kleinrahm, R. Span, M. Richter, J. Chem. Thermodyn. (2020). <https://doi.org/10.1016/j.jct.2019.106002>
6. P. Eckmann, N. von Preetzmann, G. Cavuoto, R. Kleinrahm, M. Richter, Int. J. Thermophys. (2020). <https://doi.org/10.1007/s10765-020-02728-2>
7. G. Cavuoto, N. von Preetzmann, P. Eckmann, J. Li, A.M.H. van der Veen, R. Kleinrahm, M. Richter, Int. J. Thermophys. (2021). <https://doi.org/10.1007/s10765-020-02791-9>
8. E.W. Lemmon, R.T. Jacobsen, S.G. Penoncello, D.G. Friend, J. Phys. Chem. Ref. Data (2000). <https://doi.org/10.1063/1.1285884>
9. O. Kunz, W. Wagner, J. Chem. Eng. Data (2012). <https://doi.org/10.1021/je300655b>
10. International Organization for Standardization, *ISO 20765–2:2015, Natural gas — Calculation of Thermodynamic Properties* (2015)
11. W. Wagner, R. Kleinrahm, Metrologia (2004). <https://doi.org/10.1088/0026-1394/41/2/S03>
12. M.O. McLinden, in *Volume Properties*. ed. by E. Wilhelm, T. Letcher (Royal Society of Chemistry, Cambridge, 2015)
13. D. Lozano-Martín, M.E. Mondéjar, J.J. Segovia, C.R. Chamorro, Measurement (2020). <https://doi.org/10.1016/j.measurement.2019.107176>
14. W.M. Haynes, D.R. Lide, T.J. Bruno (eds.), *CRC Handbook of Chemistry and Physics*, 97th edn. (CRC Press, Boca Raton, 2016)
15. N. Pieperbeck, R. Kleinrahm, W. Wagner, M. Jaeschke, J. Chem. Thermodyn. (1991). [https://doi.org/10.1016/S0021-9614\(05\)80295-2](https://doi.org/10.1016/S0021-9614(05)80295-2)
16. International Organization for Standardization (ISO), *ISO/IEC Guide 98–3:2008, Uncertainty of measurement – Part 3*., Geneva (2008)
17. R. Span, R. Beckmüller, S. Hielscher, A. Jäger, E. Mickoleit, T. Neumann, S. Pohl, B. Semrau, M. Thol, *TREND - Thermodynamic Reference and Engineering Data 5.0* (Lehrstuhl für Thermodynamik, Ruhr-Universität Bochum 2020)
18. A. Michels, T. Wassenaar, J.M. Levelt, W. de Graaff, Appl. sci. Res. **4**, 381 (1954)
19. A. Michels, T. Wassenaar, W. van Seventer, Appl. sci. Res. **4**, 52 (1954)
20. H. Romberg, VDI-Forsch.-Heft, Düsseldorf, VDI-Verlag, Number 543 (1971)
21. W. Blanke, Doctoral Thesis, Ruhr-Universität Bochum, 1973
22. J.B. Howley, J.W. Magee, W.M. Haynes, Int. J. Thermophys. (1994). <https://doi.org/10.1007/BF01447100>
23. O. Kunz, R. Klimeck, W. Wagner, M. Jaeschke, *The GERG-2004 Wide-Range Equation of State for Natural Gases and Other Mixtures* (GERG technical monograph 15 (2007), Fortsch.-Ber. VDI, Reihe 6, Nr. 557, VDI-Verl., Düsseldorf, 2007)
24. W. Blanke, Forsch. Ing.-Wes. (1976). <https://doi.org/10.1007/BF02573843>
25. W. Wagner, R. Kleinrahm, X. Guo, G. Olbricht, Proc. of the 1992 Int. Gas Res. Conference 863 (1992)
26. M. Richter, R. Kleinrahm, J. Chem. Thermodyn. (2014). <https://doi.org/10.1016/j.jct.2014.03.020>
27. M. Richter, M.O. McLinden, J. Chem. Eng. Data (2014). <https://doi.org/10.1021/je500792x>
28. M. Richter, M.O. McLinden, Sci. Rep. (2017). <https://doi.org/10.1038/s41598-017-06228-6>
29. X. Yang, M. Richter, Ind. Eng. Chem. Res. (2020). <https://doi.org/10.1021/acs.iecr.9b06753>
30. M.O. McLinden, C. Lössch-Will, J. Chem. Thermodyn. (2007). <https://doi.org/10.1016/j.jct.2006.09.012>

Publisher's Note Springer Nature remains neutral with regard to jurisdictional claims in published maps and institutional affiliations.

Authors and Affiliations

Nils von Preetzmann¹  · Reiner Kleinrahm¹ · Philipp Eckmann² ·
Giuseppe Cavuoto³ · Markus Richter² 

¹ Faculty of Mechanical Engineering, Thermodynamics, Ruhr University Bochum, Bochum, Germany

² Department of Mechanical Engineering, Applied Thermodynamics, Chemnitz University of Technology, Chemnitz, Germany

³ Istituto Nazionale Di Ricerca Metrologica (INRiM), Turin, Italy